

Substrate Doping Effect and Unusually Large Angle van Hove Singularity Evolution in Twisted Bi- and Multilayer Graphene

Han Peng, Niels B. M. Schröter, Jianbo Yin, Huan Wang, Ting-Fung Chung, Haifeng Yang, Sandy Ekahana, Zhongkai Liu, Juan Jiang, Lexian Yang, Teng Zhang, Cheng Chen, Heng Ni, Alexey Barinov, Yong P. Chen, Zhongfan Liu, Hailin Peng, and Yulin Chen*

Graphene has demonstrated great potential in new-generation electronic applications due to its unique electronic properties such as large carrier Fermi velocity, ultrahigh carrier mobility, and high material stability. Interestingly, the electronic structures can be further engineered in multilayer graphene by the introduction of a twist angle between different layers to create van Hove singularities (vHSs) at adjustable binding energy. In this work, using angle-resolved photoemission spectroscopy with sub-micrometer spatial resolution, the band structures and their evolution are systematically studied with twist angle in bilayer and trilayer graphene sheets. A doping effect is directly observed in graphene multilayer system as well as vHSs in bilayer graphene over a wide range of twist angles (from 5° to 31°) with wide tunable energy range over 2 eV. In addition, the formation of multiple vHSs (at different binding energies) is also observed in trilayer graphene. The large tuning range of vHS binding energy in twisted multilayer graphene provides a promising material base for optoelectrical applications with broadband wavelength selectivity from the infrared to the ultraviolet regime, as demonstrated by an example application of wavelength selective photodetector.

Graphene is a 2D honeycomb carbon crystal that exhibits unusual electronic structures and physical properties^[1–4] that make it attractive for high-performance devices, such as transistors,^[5–8] optical modulators,^[9,10] and photodetectors.^[9,11] Compared to single layer graphene, when two or more layers of graphene are stacked together with a twist angle, their electronic structure can be further enriched, giving rise to the van Hove singularity (vHS) with greatly enhanced carrier density of states, thus leading to enhanced optical absorption for selective photon energies.^[12–18] With large tuning range of the twist angle and vHS binding energy, twisted bi- and multilayer graphene provide a promising material base for fabricating broad band wavelength-selective ultrafast photodetectors from the infrared to the ultraviolet regime.


H. Peng, N. B. M. Schröter, Dr. H. F. Yang, S. Ekahana, C. Chen, H. Ni, Prof. Y. L. Chen
Department of Physics
University of Oxford
Parks Road, Oxford OX1 3PU, UK
E-mail: Yulin.Chen@physics.ox.ac.uk

Dr. J. B. Yin, Dr. H. Wang, Prof. Z. F. Liu, Prof. H. L. Peng
Center for Nanochemistry
Beijing Science and Engineering Center for Nanocarbons
Beijing National Laboratory for Molecular Sciences
College of Chemistry and Molecular Engineering
Peking University
Beijing 100871, P. R. China
T.-F. Chung, Prof. Y. P. Chen
Department of Physics and Astronomy
Birck Nanotechnology Center, and School of Electrical
and Computer Engineering
Purdue University
West Lafayette, IN 47907, USA

Dr. H. F. Yang, Prof. Z. K. Liu, Dr. J. Jiang, Prof. Y. L. Chen
School of Physical Science and Technology
ShanghaiTech University and CAS-Shanghai Science Research Center
Shanghai, China

Prof. L. X. Yang, T. Zhang, Prof. Y. L. Chen
State Key Laboratory of Low Dimensional Quantum Physics
Collaborative Innovation Center of Quantum Matter
and Department of Physics
Tsinghua University
Beijing 100084, China

Dr. A. Barinov
Elettra-Sincrotrone Trieste ScPA
Trieste 34149, Italy

 The ORCID identification number(s) for the author(s) of this article can be found under <http://dx.doi.org/10.1002/adma.201606741>.

DOI: 10.1002/adma.201606741

However, despite the consensus about the existence of vHSs for small twist angles ($\leq 5^\circ$),^[17–22] the formation of vHS for large twist angles is still under debate. Although scanning tunneling microscopy (STM) studies found that two layers with larger twist angle (5.5° in ref. [21] and 20° in ref. [22], respectively) decouple and the electronic structure becomes indistinguishable from monolayer graphene, recent optical and theoretical studies suggest that the vHSs may persist at large twist angles up to 30° .^[18,19,23–25] To settle this discrepancy, it is highly required to systematically and directly investigate the electronic structure of twisted bi- and multilayer graphene over a wide twist angle regime.

Angle-resolved photoemission spectroscopy (ARPES) has been a powerful tool to study the band structure of crystals, including graphene.^[26,27] However, the poor spatial resolution (typically hundreds of micrometers) makes it unsuitable for the systematic study of the electronic structure of twisted bi- and multilayer graphene, as their grain size is typically up to tens of micrometers. Fortunately, the recent development of ARPES with sub-micrometer spatial resolution (i.e., micro-ARPES)^[28,29] provides an excellent tool for this study. The capability of obtaining complete electronic structures of samples down to $1\ \mu\text{m}$ enables us to investigate and to compare graphene domains with varying twist angles.

In this work, we apply the micro-ARPES to study the multilayer graphene sheets and observe a doping effect in this

multilayer system. We then systematically study the twist angle evolution of vHS in the twisted bi- and trilayer graphene. We observe not only the vHSs in twisted bilayer graphene (tBLG) over a wide range of twist angle (from 5° to 31°), but also coexistence of multiple vHSs at different energies in twisted trilayer graphene (tTGL). Our result suggests that the interlayer coupling persists at large twist angles. This discovery allows one to tune the binding energy of the vHS up to over 2 eV, thus leading to a promising application in wavelength-selective ultrafast photodetection from infrared to ultraviolet regime. We demonstrate this application by a proof-of-principle photodetector with a much enhanced photocurrent generation at the photon energy that matches the binding energy of the vHS.

First, we show the applicability of micro-ARPES in investigating multilayer graphene. The principle of micro-ARPES is illustrated in **Figure 1a**, where the photon beam from the synchrotron beamline is focused onto the sample down to a spot size less than $1\ \mu\text{m}$ in diameter ($\approx 0.8\ \mu\text{m}$ ^[28,29]). At a given sample position, the electron analyzer can rotate around two axes to collect the 3D electronic band structure; and the sample can be scanned in two directions, thus the band structure at different sample locations can be investigated.

Due to the ultrathin nature of each graphene layer ($\approx 3.3\ \text{\AA}$) and the relatively large penetration depth of the photon beam,^[30] micro-ARPES is an ideal tool for the study of single- and multilayer graphene, as the photoelectrons from the

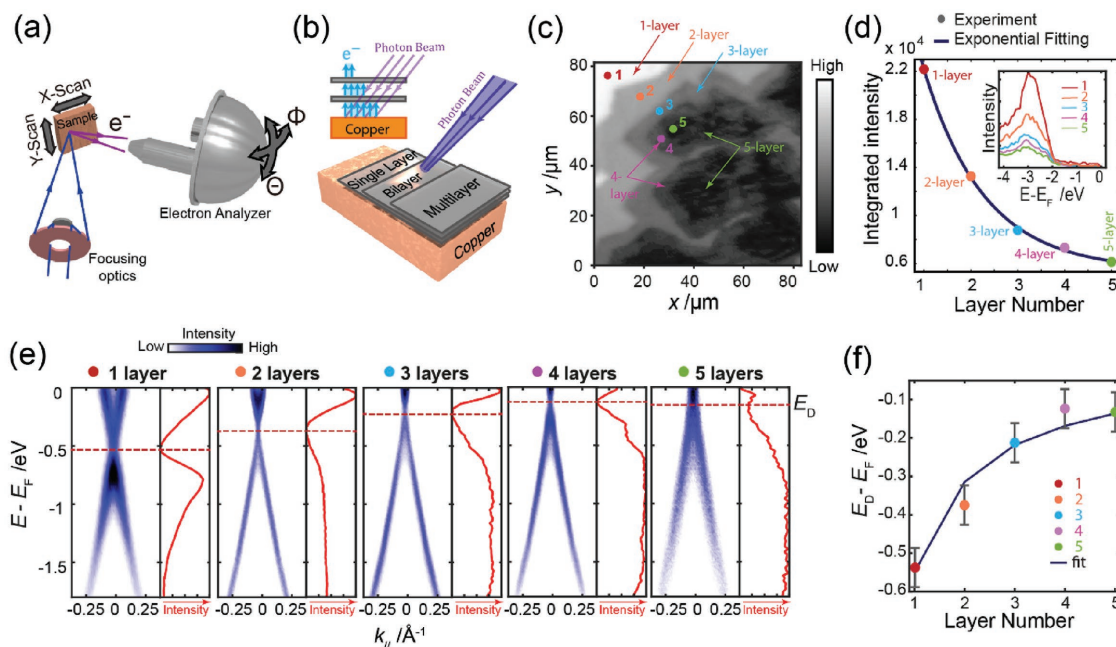


Figure 1. Micro-ARPES measurements of multilayer graphene. a) Illustration of micro-ARPES operational principle. Rotating the analyzer probes along Θ and Φ direction different momenta in reciprocal space, while moving the sample probes along X and Y direction different positions in real space. Either a Schwarzschild mirror (as shown here) or a Fresnel zone plate achieves microfocusing of the synchrotron light. b) Illustration of ARPES spatial scanning of multilayer graphene on copper foil substrate. The inset shows the absorption of photoelectrons from the copper d-bands for consecutive graphene layers. c) Large-scale spatial scanning image of the sample in the spectral range of the copper d-bands. Dots with different color mark selected positions for subsequent measurement. d) Integrated intensity from the positions marked with the dot of corresponding color, plotted over layer number, and exponential fitting curve (dark blue line). The respective integrated energy distribution curves (EDCs) are presented in the inset. e) Energy–momentum–dispersion taken at positions shown in (c). Red dashed lines indicate the energy of the Dirac point (E_D) in each spectrum of the top layer. Red solid curves are integrated EDCs for each spectrum, which are corrected by the Fermi–Dirac distribution, allowing to see features near the Fermi surface. f) Evolution of E_D of the top layer with total number of layers. The blue line indicates a fit of the data using the capacitor-model outlined in Figure 2.

substrate and different graphene layers can be studied simultaneously in the same measurement, as illustrated in Figure 1b.

Figure 1c,d demonstrates an example how micro-ARPES can be used to study multilayer graphene and determine the photoelectron penetration depth: graphene containing one- to five-layer domains grown by chemical vapor deposition (CVD) on copper foil (Figure 1c, and see the Experimental Section for more details) are measured with micro-ARPES. We first scan the samples and record the spectral intensity map of photoelectrons from the Cu d-bands, which are attenuated differently depending on the thickness of the overlaying graphene multilayer (Figure 1b,c). The intensity map (Figure 1c) shows clear contrast on —one- to five-layer of graphene across the sample. A more quantitative analysis of the integrated photoelectron intensity is shown in Figure 1d, illustrating an exponential decay with the increasing number of the overlaying graphene layers. The fitting to the curve with a simple model $I = I_0 e^{-x/\lambda} + I_1$ (Figure 1d, x is the layer number and I_0 and I_1 are fitting constants) yields that the average photoelectron penetration depth is $\lambda = 1.3$ graphene layers, indicating that micro-ARPES is capable of the study of multilayer graphene up to five layers with 5% intensity from the bottom layer.

Exploiting the capability to identify graphene domains with different thicknesses, we directly observe the substrate doping effect on multilayer graphene. As can be seen in Figure 1e, with increasing number of layers, the top layer of graphene becomes less electron-doped, which we could explain by an effective capacitor model of the multilayer system^[31] (Figure 1f). The details of the model are illustrated in Figure 2: due to the existence of an effective work function difference caused by chemical interactions, the electrons will transfer from the copper substrate to graphene, filling the unoccupied states (Figure 2a), which will result in the doping effect.^[31] These transferred electrons form an electric field and, as a result, balance the effective potential difference. As the graphene layer increases, the top layers are shielded from the substrate, and hosts less transferred electrons than the lower layers (Figure 2b). A quantitative analysis of the model is presented in Figure S1

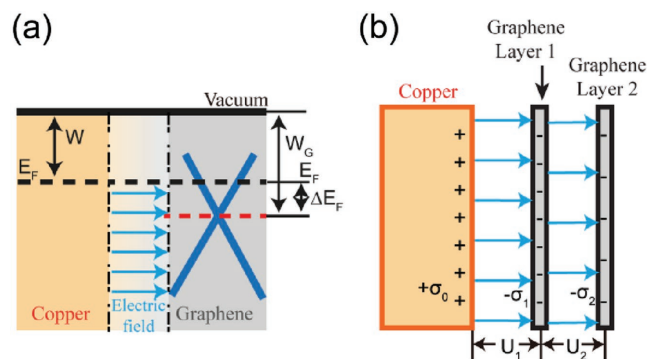


Figure 2. Effective capacitor model for the graphene band's doping level. a) Illustration for the effective capacitor model. Due to the charge transfer, there is an electric field between copper substrate and graphene layer, which leads to a shift ΔE_F of the Dirac cone to higher binding energies. W_C is the work function of freestanding graphene, and W the work function of the whole system. b) Illustration of the model for the two-layer case. $-\sigma_{1/2}$ is the transferred charge per unit area for the graphene layer 1/layer 2, while σ_0 is for the copper substrate.

(Supporting Information) and the fitting result is shown in Figure 1f.

We note the electrons from lower graphene layers are not found in Figure 1e as they are either too weak or outside the detection window, but at some domains of twisted bi- and multilayer graphene we could detect multiple Dirac cones from each layer, which allow us to observe the vHS when the Dirac cones are intersecting.

After illustrating the applicability, we now apply micro-ARPES to the systematic study of bi- and multilayer graphene and search for vHSs over a broad twist angle range. Figure 3 demonstrates a typical morphology and spectrum of twisted multilayer graphene with variable twist angles. The optical microscope image (Figure 3a) as well as the spatially ARPES scanning (Figure 3b) clearly shows the graphene domains on the Cu substrate. Especially, the spatially ARPES scanning results show much better contrast that enables us to differentiate the layer number in the graphene domains (Figure 3b(iii)), which allows the further measurement of thickness dependent electronic band structure.

From the alignment of the edges of different layers shown in Figure 3b(iii), we can already see that layer 1 and layer 2 are twisted. Indeed, the measurement of the electronic structure at point P1 (see Figure 3b(iii)) shows a typical band dispersion (Figure 3c,d) of twisted bilayer graphene, which displays two Dirac cones shifted in momentum space due to a twist angle of 8.2° . (The spectrum of Dirac cone from the lower layer is weaker due to the depth attenuation effect discussed in Figure 1d.) When the two Dirac cones intersect, they hybridize and open up a gap, forming the vHS at the saddle point, which can be seen both in the constant energy band contours (Figure 3c) and the dispersions (Figure 3d). From the dispersions and the corresponding integrated energy distribution curve, we can also see that the vHS provides large density of states near the gap (Figure 3d). In addition to the gap opened at the crossing point, mini gaps are observed in the equal energy contours (green arrows in the middle panel) due to a Moiré superpotential (see more discussions in Figure S2, Supporting Information). In Figure 3b(iii), the bottom two layers (layer 2 and layer 3) appear to be well aligned geometrically, while the top layer (layer 1) is twisted. The stacking order of the layers is discussed Section 3 of the Supporting Information.

We then focus on the bilayer graphene domains and investigate the relationship between the twist angle and the binding energy of vHSs, a few examples are shown in Figure 4a and more results are summarized in Figure 4c ranging from 5° to 31° . The evolution of the vHS binding energy can be well reproduced by a theoretical model (Figure 4b)^[23] (note that the deviation from a linear relationship between vHS binding energy and twist angle stems from the nonlinearity of the graphene electronic band structure at large binding energies, a detailed discussion and the theoretical model can be found in Figure S5, Supporting Information). Recent theoretical and transport studies also reported a band gap opening at the Dirac points.^[32–36] However, due to slightly curved sample surface (caused by the substrate) that mixes the dispersion of different angles (thus different k-space locations) and the limited energy resolution, the suggested band gap is not clearly observed in the present study, which will be investigated in our follow-up

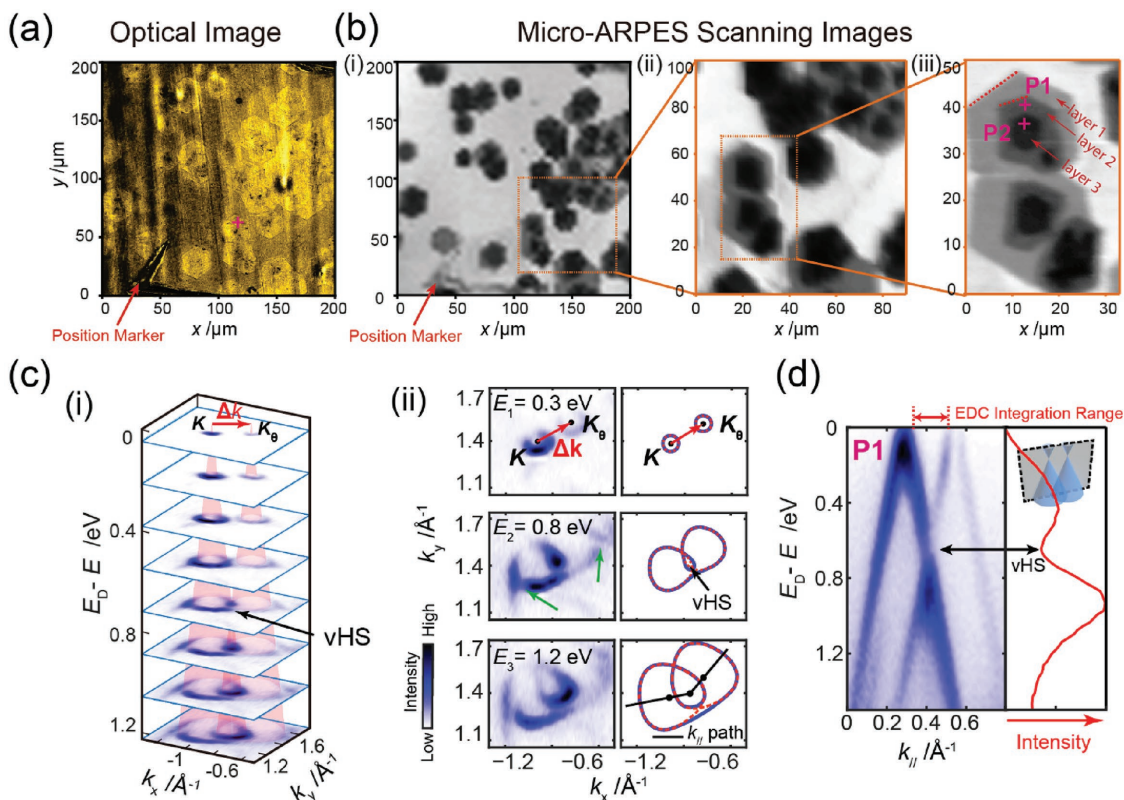


Figure 3. Typical twisted multilayer graphene morphology and spectrum. a) Optical microscope image of the bilayer graphene sample to identify the region of interest. The pink crosses indicate where subsequent micro-ARPES measurements were taken. b) (i)–(iii) Spatial scanning images of the region of interest with increasing magnification. To achieve higher resolution, finer scanning steps were adopted. c) (i) Equal energy contours of tBLG band structure with twist angle 8.2° measured at P1, which is marked in (b), showing two Dirac cones. (ii) Comparison between measured and illustrating energy contours. The dotted red curves are calculated from a tight binding model for the overlapping bands from two Dirac cones without hybridization. The solid blue curves show a guide to the eye to illustrate the hybridization effect. The mini gaps marked by green arrows stem from a Moiré superpotential, which is further discussed in Figure S2 (Supporting Information). d) Energy–momentum–dispersion measured at P1 passing through the two Dirac points and the van Hove singularity (k_y path is indicated in the bottom of Figure 3c(ii)). The right panel shows the integrated EDC over the region shown above. The energy–momentum–dispersion of twisted trilayer graphene, measured at P2 (which is marked in (b)), is shown in Figure S3 (Supporting Information).

works. In addition to the data from bilayer graphene, Figure 4c also shows the binding energies for the two vHSs in twisted trilayer graphene (blue symbols), which will be discussed in the last section.

Given the greatly enhanced carrier density of states at the vHS binding energy, it is possible to design a photodetector that is most sensitive to a certain wavelength ($E_{\text{photon}} = 2E_{\text{vHS}}$). Furthermore, the broad tunability of the vHS binding energy (by changing the twist angle) demonstrated from our measurements (up to 2.5 eV, see Figure 4c) guarantees the broad operation range from infrared to ultraviolet (up to 5 eV) photons.

A proof-of-concept device has been fabricated to demonstrate such application, as illustrated in Figure 4d. We pattern two bilayer graphene domains with different twist angles of 13° and 6° (corresponding to the $2E_{\text{vHS}}$ of 2.3 and 1.1 eV, respectively). We then scan a focused laser beam (532 nm, $E_{\text{photon}} = 2.3$ eV) with spot size of $\approx 1 \mu\text{m}$ over the device, while the induced short-circuit photocurrent is recorded as a function of laser spot positions. Remarkably, in region 1 (13° twist angle) where the resonance absorption condition ($E_{\text{photon}} = 2 E_{\text{vHS}} = 2.3$ eV) is met, the photocurrent is greatly enhanced (by 600%) compared

to region 2 (6° twist angle), clearly demonstrating the feasibility and potential of the wavelength-selection application.

As discussed above, twisted trilayer graphene (tTLG) is observed from spatial scanning image and further investigated by ARPES measurement. Typical tTLG observed in the experiment presents a Twist-A-B structure (Figure 5a), in which the bottom two graphene layers are A-B stacked bilayer,^[37] with top layer twisted. As illustrated in Figure 5b, the dispersions are composed of a single Dirac cone dispersion (on the left, originated from the top layer) and a double layer graphene dispersion with weaker intensity (on the right, originated from the bottom A-B stack). An apparent gap between the conduction and valence band from the A-B stack is opened due to the existence of the electric potential difference across the A-B stacked layers,^[37,38] which is a result from the capacitor effect (detailed discussion can be found in Figure S1, Supporting Information). More interestingly, the ARPES measurement in Figure 5c shows that at the crossing points of the single layer (layer 1) and the bilayer (layer 2, 3) dispersion, two vHSs are formed, as is observable both in the band dispersion plot and the spectral intensity plot (Figure 5c(ii)). The two vHSs present a separation

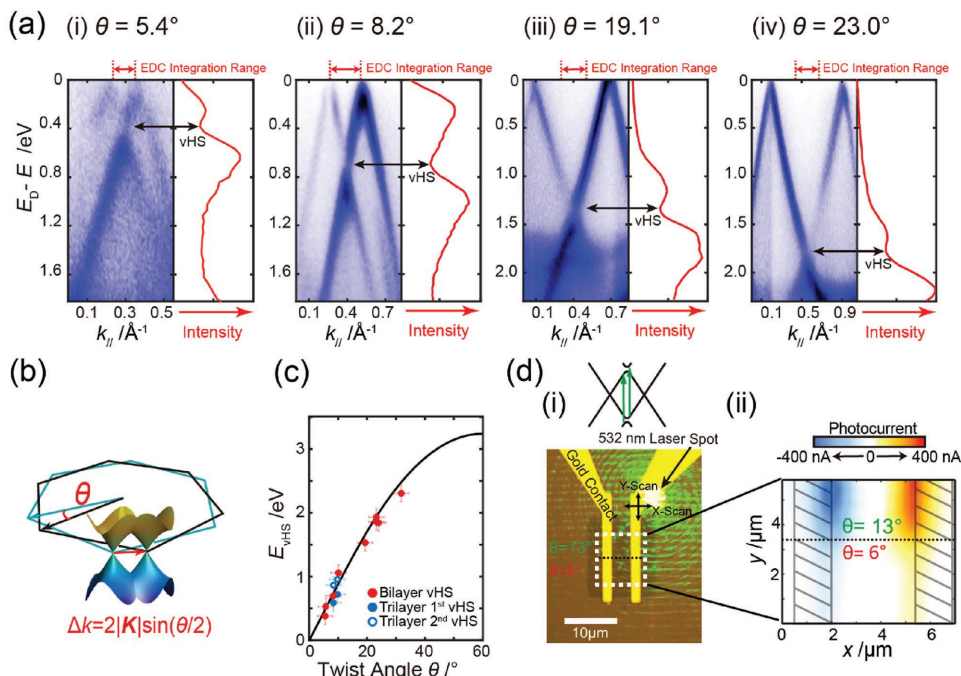


Figure 4. Evolution of van Hove singularity binding energy with twist angle. a) Energy–momentum–dispersion for typical twist angles 5.4° , 8.2° , 19.1° , and 23.0° , respectively. Data sets from more angles are presented in Figure S4 (Supporting Information). b) Illustration of the relationship between the measured Δk and the calculated twist angle θ . As θ increases, the separation of two Dirac cones from each layer increases as well, which results in larger banding energy of vHS (the crossing point). c) Relationship between twist angle and E_{vHS} ; the red and blue dots indicate the experimental results, while the black line is the predicted evolution by the theoretical model (for more details, see Figure S5, Supporting Information), showing the nonlinearity of the vHS binding energy at large twist angles. d) Photodetector showing large photocurrent under the illumination of corresponding wavelength due to the vHS binding energy. (i) Optical image of the device with two regions of tBLG with varying twist angle under the illumination of a 532 nm laser. The insets show that the vHS pair will result in large response to the impeding laser with the photon energy that double the vHS binding energy. (ii) Real space mapping of the photocurrent during illumination. The two twist angle regions respond differently to the excitation wavelength.

of ≈ 0.2 eV, as is expected from the separation between two bands in A-B stacked graphene.^[3]

Our experimental results clearly establish that interlayer coupling between graphene layers is present over a broad twist angle (up to 31°), thus greatly extending the range (1° – 10°)

of interlayer coupling suggested by previous scanning tunneling microscopy (STM)/scanning tunneling spectroscopy (STS) studies.^[19] We also note that the large angle coupling reported here stands in contrast to some STM/STS studies^[21,22] that report the disappearance of vHSs above a twist angle of

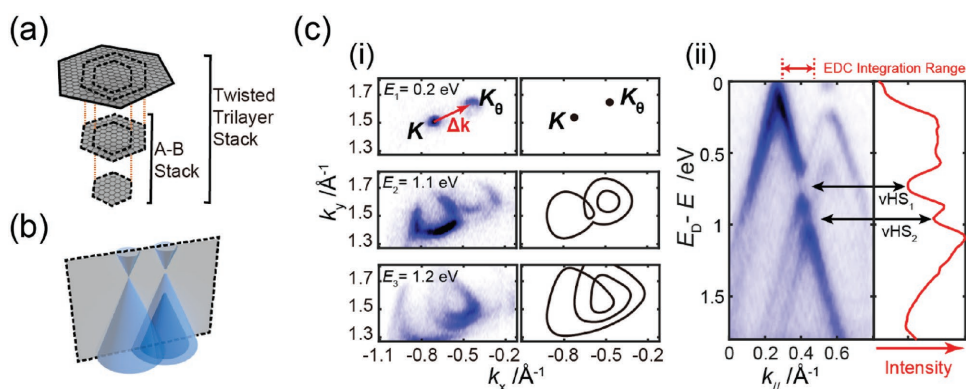


Figure 5. van Hove singularities in twisted trilayer graphene. a) Lattice structure illustration for twisted trilayer graphene (tTLG). We expect the smaller layers to lie below the bigger ones, as was reported in ref. [39]. b) Illustration of tTLG band structure. The left cone originates from the twisted top layer. The right double cone originates from the A-B stacked middle and under layers. c) (i) The left panel shows equal energy contours for the tTLG band structure data, with the illustration for the band structure in the right panel. (ii) Energy–momentum–dispersion of tTLG band structure, with cutting direction as shown by the gray plane in (b). The right panel shows integrated EDC over the region shown above. The tTLG dispersion presents two van Hove singularities with a difference in binding energy of ≈ 0.2 eV.

5.5° and 20°, respectively. The difference in the findings may result from different sample quality and/or the differences in the measurement positions (more discussions can be found in Figure S6, Supporting Information).

On the other hand, recent optical studies also reported enhanced absorption and optical conductivity at energies that could correspond to the VHS binding energy at large twist angles,^[17,18,23] however, there is a competing interpretation for these optical results, which is based on optical enhancement by parallel bands of two twisted Dirac cones^[23] and does not require the existence of vHS. Thus our study constitutes the first direct evidence for the existence of the vHS in twisted bi- and multilayer graphene at large twist angles. In addition to the interlayer coupling at large twist angle, we also demonstrated that bi- and multilayer graphene could be used in wavelength selective photodetection, thus open up the door for applying twisted bi- and multilayer graphene in optoelectronic applications ranging from the infrared to the ultraviolet regime.

Experimental Section

Twisted few-layer graphene samples were grown on copper foil via CVD.^[40] micro-ARPES was performed at the spectromicroscopy beamline at the Elettra synchrotron in Trieste, Italy.^[28] The measurements were done under a base pressure of 10⁻¹⁰ mbar in ultrahigh vacuum and the sample kept at the temperature 110 K to minimize the thermal broadening of the spectra. The spectra were taken at a photon energy of 74 eV in Elettra, with estimated energy and angular resolution of ≈50 meV and ≈0.5°, respectively. Before transferring into the photoemission acquisition chamber, the samples was annealed at 350 °C for 30 min in a preparation chamber with base pressure 10⁻¹⁰ mbar to remove H₂O and other contaminants adsorbed during the transfer in air.

All data needed to evaluate the conclusions in the paper are present in the paper and/or the Supporting Information. Additional data related to this paper may be requested from the authors.

Supporting Information

Supporting Information is available from the Wiley Online Library or from the author.

Acknowledgements

H.P. and N.B.M.S. contributed equally to this work. The authors are grateful to Dr. J. J. Jia for help in ARPES experiment at Elettra. The authors thank Y. T. Zhang from Nanjing University, for the discussion and help in data analysis. Y.L.C. acknowledges the support from the EPSRC (UK) Platform Grant (Grant No. EP/M020517/1), and Hefei Science Center CAS (2015HSC-UE013). H.P. and C.C. acknowledge the support from China Scholarship Council. N.B.M.S. acknowledges the support from Studienstiftung des deutschen Volkes. Y.L.C. conceived the experiments; H.P. and N.B.M.S. carried out ARPES measurements with the assistance of A.B., Z.K.L., J.J., T.Z., C.C., H.F.Y., L.X.Y., and S.E.; H.P. analyzed ARPES data with the assistance of N.B.M.S. and H.N.; J.B.Y., H.W., H.L.P., Z.F.L., T.F.C., and Y.P.C. performed the synthesis; J.B.Y. made the devices and carried out optoelectronic measurements; H.P., N.B.M.S., and J.B.Y. wrote the paper. All authors contributed to the scientific planning and discussions. The authors declare that they have no competing interests.

Keywords

micro-ARPES, substrate doping effect, twisted bilayer graphene, van Hove singularity

Received: December 13, 2016

Revised: January 22, 2017

Published online: May 8, 2017

- [1] K. Novoselov, A. K. Geim, S. Morozov, D. Jiang, M. Katsnelson, I. Grigorieva, S. Dubonos, A. Firsov, *Nature* **2005**, 438, 197.
- [2] Y. Zhang, Y.-W. Tan, H. L. Stormer, P. Kim, *Nature* **2005**, 438, 201.
- [3] A. H. Castro Neto, N. M. R. Peres, K. S. Novoselov, A. K. Geim, *Rev. Mod. Phys.* **2009**, 81, 109.
- [4] A. Rozhkov, A. Sboychakov, A. Rakhmanov, F. Nori, *Phys. Rep.* **2016**, 648, 1.
- [5] X. Wang, X. Li, L. Zhang, Y. Yoon, P. K. Weber, H. Wang, J. Guo, H. Dai, *Science* **2009**, 324, 768.
- [6] P. Avouris, *Nano Lett.* **2010**, 10, 4285.
- [7] L. Liao, Y.-C. Lin, M. Bao, R. Cheng, J. Bai, Y. Liu, Y. Qu, K. L. Wang, Y. Huang, X. Duan, *Nature* **2010**, 467, 305.
- [8] F. Schwierz, *Nat. Nanotechnol.* **2010**, 5, 487.
- [9] F. Bonaccorso, Z. Sun, T. Hasan, A. C. Ferrari, *Nat. Photonics* **2010**, 4, 611.
- [10] M. Liu, X. Yin, E. Ulin-Avila, B. Geng, T. Zentgraf, L. Ju, F. Wang, X. Zhang, *Nature* **2011**, 474, 64.
- [11] F. Xia, T. Mueller, Y. M. Lin, A. Valdes-Garcia, P. Avouris, *Nat. Nanotechnol.* **2009**, 4, 839.
- [12] J. M. B. Lopes dos Santos, N. M. R. Peres, A. H. Castro Neto, *Phys. Rev. Lett.* **2007**, 99, 256802.
- [13] G. Li, A. Luican, J. M. B. Lopes dos Santos, A. H. Castro Neto, A. Reina, J. Kong, E. Y. Andrei, *Nat. Phys.* **2009**, 6, 109.
- [14] W. Landgraf, S. Shallcross, K. Türschmann, D. Weckbecker, O. Pankratov, *Phys. Rev. B* **2013**, 87, 075433.
- [15] S. Shallcross, S. Sharma, O. Pankratov, *Phys. Rev. B* **2013**, 87, 245403.
- [16] T. Ohta, J. T. Robinson, P. J. Feibelman, A. Bostwick, E. Rotenberg, T. E. Beechem, *Phys. Rev. Lett.* **2012**, 109, 186807.
- [17] P. Moon, M. Koshino, *Phys. Rev. B* **2013**, 87, 205404.
- [18] R. W. Havener, Y. Liang, L. Brown, L. Yang, J. Park, *Nano Lett.* **2014**, 14, 3353.
- [19] I. Brihuega, P. Mallet, H. Gonzalez-Herrero, G. Trambly de Laissardiere, M. M. Ugeda, L. Magaud, J. M. Gomez-Rodriguez, F. Yndurain, J. Y. Veuillein, *Phys. Rev. Lett.* **2012**, 109, 196802.
- [20] K. Uchida, S. Furuya, J.-I. Iwata, A. Oshiyama, *Phys. Rev. B* **2014**, 90, 155451.
- [21] W. Yan, L. Meng, M. Liu, J.-B. Qiao, Z.-D. Chu, R.-F. Dou, Z. Liu, J.-C. Nie, D. G. Naugle, L. He, *Phys. Rev. B* **2014**, 90, 115402.
- [22] A. Luican, G. Li, A. Reina, J. Kong, R. R. Nair, K. S. Novoselov, A. K. Geim, E. Y. Andrei, *Phys. Rev. Lett.* **2011**, 106, 126802.
- [23] R. W. Havener, H. Zhuang, L. Brown, R. G. Hennig, J. Park, *Nano Lett.* **2012**, 12, 3162.
- [24] K. Kim, S. Coh, L. Z. Tan, W. Regan, J. M. Yuk, E. Chatterjee, M. F. Crommie, M. L. Cohen, S. G. Louie, A. Zettl, *Phys. Rev. Lett.* **2012**, 108, 246103.
- [25] R. He, T. F. Chung, C. Delaney, C. Keiser, L. A. Jauregui, P. M. Shand, C. C. Chancey, Y. Wang, J. Bao, Y. P. Chen, *Nano Lett.* **2013**, 13, 3594.
- [26] M. Sprinkle, D. Siegel, Y. Hu, J. Hicks, A. Tejada, A. Taleb-Ibrahimi, P. Le Fèvre, F. Bertran, S. Vizzini, H. Enriquez, S. Chiang, P. Soukiassian, C. Berger, W. A. de Heer, A. Lanzara, E. H. Conrad, *Phys. Rev. Lett.* **2009**, 103, 226803.

- [27] S. Y. Zhou, G. H. Gweon, A. V. Fedorov, P. N. First, W. A. de Heer, D. H. Lee, F. Guinea, A. H. Castro Neto, A. Lanzara, *Nat. Mater.* **2007**, *6*, 770.
- [28] P. Dudin, P. Lacovig, C. Fava, E. Nicolini, A. Bianco, G. Cautero, A. Barinov, *J. Synchrotron Radiat.* **2010**, *17*, 445.
- [29] J. Avila, I. Razado-Colambo, S. Lorcy, B. Lagarde, J.-L. Giorgetta, F. Polack, M. C. Asensio, *J. Phys.: Conf. Ser.* **2013**, *425*, 192023.
- [30] M. Seah, W. Dench, *Surf. Interface Anal.* **1979**, *1*, 2.
- [31] G. Giovannetti, P. A. Khomyakov, G. Brocks, V. M. Karpan, J. van den Brink, P. J. Kelly, *Phys. Rev. Lett.* **2008**, *101*, 026803.
- [32] E. J. Mele, *Phys. Rev. B* **2010**, *81*, 161405.
- [33] Z. Ni, L. Liu, Y. Wang, Z. Zheng, L.-J. Li, T. Yu, Z. Shen, *Phys. Rev. B* **2009**, *80*, 125404.
- [34] J. Park, W. C. Mitchel, S. Elhamri, L. Grazulis, J. Hoelscher, K. Mahalingam, C. Hwang, S.-K. Mo, J. Lee, *Nat. Commun.* **2015**, *6*, 5677.
- [35] A. V. Rozhkov, A. O. Sboychakov, A. L. Rakhmanov, F. Nori, *Phys. Rev. B* **2017**, *95*, 045119.
- [36] A. O. Sboychakov, A. L. Rakhmanov, A. V. Rozhkov, F. Nori, *Phys. Rev. B* **2015**, *92*, 075402.
- [37] T. Ohta, A. Bostwick, T. Seyller, K. Horn, E. Rotenberg, *Science* **2006**, *313*, 951.
- [38] E. V. Castro, K. Novoselov, S. Morozov, N. Peres, J. L. Dos Santos, J. Nilsson, F. Guinea, A. Geim, A. C. Neto, *Phys. Rev. Lett.* **2007**, *99*, 216802.
- [39] S. Nie, W. Wu, S. Xing, Q. Yu, J. Bao, S.-S. Pei, K. F. McCarty, *New J. Phys.* **2012**, *14*, 093028.
- [40] C. Mattevi, H. Kim, M. Chhowalla, *J. Mater. Chem.* **2011**, *21*, 3324.